Electrochimica Acta 261 (2018) 236–245

Contents lists available at ScienceDirect

Electrochimica Acta

journal homepage: www.elsevier.com/locate/electacta

Bio-template synthesized NiO/C hollow microspheres with enhanced Li-ion battery electrochemical performance

Jiangyang Tian [a], Qian Shao [a, *], Xiaojie Dong [a], Jinlong Zheng [b], Duo Pan [a], Xiyu Zhang [a], Huili Cao [c], Luhan Hao [d], Jiurong Liu [c, **], Xianmin Mai [e, ***], Zhanhu Guo [d, ****]

[a] College of Chemical and Environmental Engineering, Shandong University of Science and Technology, Qingdao, 266590, PR China
[b] School of Chemistry, Beihang University, Beijing, 100191, China
[c] Key Laboratory for Liquid–Solid Structural Evolution and Processing of Materials, Ministry of Education and School of Materials Science and Engineering, Shandong University, Jinan, Shandong, 250061, China
[d] Integrated Composites Laboratory (ICL), Department of Chemical & Biomolecular Engineering, University of Tennessee, Knoxville, TN 37996, USA
[e] School of Urban Planning and Architecture, Southwest Minzu University, Chengdu, 610041, China

ARTICLE INFO

Article history:
Received 5 June 2017
Received in revised form
16 November 2017
Accepted 12 December 2017
Available online 13 December 2017

Keywords:
Yeast template
NiO/C hollow microspheres
Electrochemical performance
Anode material
Li-ion batteries

ABSTRACT

NiO microspheres with well-defined hollow structure were successfully obtained using spherical yeast as a natural bio-template. The as-prepared samples were characterized by X-ray diffraction (XRD), scanning electron microscopy (SEM) and transmission electron microscopy (TEM). The morphologically uniform NiO hollow microspheres prepared with yeast template after calcination had an averaged diameter of 1.5 −2 μm and the shell thickness of ~500 nm. The concentration of $Ni(NO_3)_2$, calcination temperature and aging time play important roles on the crystal phase and morphologies of the NiO hollow microspheres. Meanwhile, the NiO/C hollow microspheres were successfully fabricated via a simple hydrothermal method using glucose as carbon source. A possible formation mechanism of forming NiO/C hollow microspheres was proposed and the electrochemical performance of the NiO/C hollow microspheres as anode material for Li-ion batteries was investigated. Compared with the samples prepared without template or without carbon coating, the as-prepared NiO/C hollow microspheres show higher discharge capacity and better cycle performance as an anode material in Li-ion batteries.

1. Introduction

The micron and nano structures with hollow interiors have attracted considerable interests in recent years due to their low density and large specific surface area [1], which endow them with great potential applications as catalysts [2], batteries [3,4], thermoelectric power generator [5], chemical sensors [6], intelligent sensing [7–10], and electromagnetic interference (EMI) shieling [11,12] in many practical fields including environmental protection [13,14], energy storage [15], catalysis [16–18], adsorption [19] and biomedicine [20]. Template-directed method [21,22], which is a traditional and simple way of producing hollow nanostructures, has been widely used. Compared with traditional templates such as polystyrene latex (PSL) [23], porous anodic aluminum oxide membrane (AAO) [24,25], $CaCO_3$ [26,27], carbon spheres [28] and carbonaceous polysaccharide microspheres [29], the biological templates [30] are economical, safe and environment friendly.

A series of methods have been developed by using microorganisms as templates for the preparation of inorganic hollow spheres. For example, Zhang et al. prepared ZnO/CdS hollow spheres by employing *Bacillus subtilis* as templates [31]. Lim et al. fabricated multiphasic hollow rods, which consisted of nanoscale Sn-based materials by using *bacillus subtilis* as templates [32]. Yang and co-workers prepared Au nanowires by employing *escherichia coli* as templates and used CTAB as the surface active agent [33]. From the above methods, it can be seen that both dead and living cells are able to bind metal cations through coordination or electrostatic attraction because of the retention of bio-functionality and active biomolecules on the cell walls. Moreover, the roughly spherical shape, renewability and enormous quantity make them good candidates as templates to form hollow spheres.

* Corresponding author.
** Corresponding author.
*** Corresponding author.
**** Corresponding author.
E-mail addresses: shaoqian01@126.com (Q. Shao), jrliu@sdu.edu.cn (J. Liu), maixianmin@foxmail.com (X. Mai), zguo10@utk.edu (Z. Guo).

https://doi.org/10.1016/j.electacta.2017.12.094
0013-4686/

Nickel oxide (NiO), an important P-type semiconductive transition metal oxide, has received considerable attention and attractive applications in various fields [34], such as catalysts [35], gas sensor materials [36], drug delivery [37] and fuel cell electrodes [38]. Especially, just like most of the transition metal oxides, it could also be used as anode materials for lithium ion batteries (LIBs) [39,40]. Compared with commercially graphite anode, these materials possessed much higher theoretical specific capacity (720 mAh g^{-1}) [41]. However, its large-scale use in LIBs is mainly limited by the large expansion in volume, serious aggregation or pulverization of active particles during charge-discharge, and its poor conductivity [42]. Many efforts have been tried to solve these problems, such as coating carbon materials, doping ions and controlling the morphologies of materials [43–45], all of these aimed to improve the structure stability or conductivity. NiO coated carbon materials were composed and applied widely in the other fields, such as Liu et al. prepared hierarchical flower-like NiO/C composite as supercapacitors [46]. Yang et al. composed NiO/C nanofiber composites derived from metal organic framework fibers as electrode materials [47].

In the present work, yeast was selected as the bio-template to control the morphologies of NiO materials. And a carbon-coating was introduced to further improve the stability of NiO. The yeast templates are known available in large quantities and easy to be produced, the reactive functional groups on the cell walls make them be a template possible [48]. To the best of our knowledge, there is no article on the synthesis and application in anode material for Li-ion batteries of NiO/C hollow microspheres prepared using yeast as the template. The NiO/C hollow microspheres were successfully obtained by using yeasts bio-template and glucose as carbon source. The as-prepared NiO/C hollow microspheres were used as anode material for Li-ion batteries. In order to test the charge/discharge capacity and cycling performance, charge-discharge measurements were carried out using a battery test system (LAND CT2001A model). The as-prepared NiO/C hollow microspheres exhibited a higher capacity and greater cycling stability compared with the samples prepared without templates or without carbon coating.

2. Experimental

2.1. Materials

Nickel nitrate hexahydrate [$Ni(NO_3)_2 \cdot 6H_2O$], ammonium hydrogencarbonate (NH_4HCO_3), glucose and absolute ethanol were provided by Tianjin Benchmark Chemical Reagent Co. Ltd. (Tianjin, China). Ethylene carbonate and diethyl carbonate were provided by Tianjin Jinniu Power Sources Material Co. Ltd. (Tianjin, China). All reagents were analytical grade and without further purification. The instant dry yeast was purchased from Angel Yeast Co. Ltd and washed with distilled water before usage.

2.2. Preparation of NiO hollow microspheres

The NiO hollow microspheres were prepared by a facile method. Typically, 0.5 g yeast was dispersed into 40 mL distilled water. Then, $Ni(NO_3)_2$ (5 mL, 0.5 M) solution was added into the above solution and stirred for 1 h at room temperature. After that, NH_4HCO_3 (5 mL, 0.5 M) solution was dropped into the reaction mixture under continuous magnetic stirring. The solution was allowed to proceed for another 1 h and then maintained at room temperature for 12 h. Finally, the products were centrifuged and washed with distilled water and ethanol for several times to remove excess reactants. After that, the products were dried at 60 °C under atmospheric conditions and calcined at 600 °C for 2 h to remove the biological cells. Thus, the NiO hollow microspheres were obtained. Meanwhile, the NiO nanoparticles were fabricated without template through the same method for comparison.

2.3. Preparation of NiO/C hollow microspheres

A simple hydrothermal method was used to synthesize NiO/C hollow microspheres. Typically, 0.3 g as-prepared NiO hollow microspheres were dispersed in a certain concentration of glucose solution (0.20 M, 30 mL) by ultrasonication and then stirred for 30 min at room temperature. Afterward, the resulting solution was sealed in a 30 mL Teflon-lined stainless steel autoclave and maintained at 180 °C for 12 h, and then cooled down naturally to room temperature. After that, the products were centrifuged and washed with distilled water and ethanol for 3 times. Finally, the NiO/C products could be acquired by calcining the obtained precursor at 600 °C for 2 h in N_2 atmosphere.

2.4. Characterizations

The crystal structures of the products were determined by XRD patterns with a X-ray diffractometer (XRD, D8 Advance, BRUKER, Germany) and 2θ ranges from 10° to 80°, using Cu Kα radiation ($\lambda = 0.1540$ nm). The morphologies and microstructures of the products were investigated by field emission scanning electron microscopy (SEM, S-4800, Hitachi, Japan) with an accelerating voltage of 30 kV and the interior hollow structure of the products could be observed by the transmission electron microscopy (TEM, JEM-1200EX, Japan). Thermal stability was studied by heating the sample in a thermogravimetric analyser (TGA, NETZSCH STA 449F3, Japan) at 10 °C min^{-1} in air atmosphere from 30 to 800 °C. The surface area were analyzed by the Brunaner-Emmett-Teller (BET) method using an BELSORP-MiniⅡapparatus (Microtrac Bel Co. Ltd, Japan).

2.5. Electrochemical measurements

In order to test the electrochemical performance of the Li-ion anode, the as-prepared active products were adjusted as 80 wt% by 10 wt% carbon black and 10 wt% polyvinylidene fluoride (PVDF) dissolved in N-methy-2-pyrrolidone (NMP) to form a slurry, which was then coated onto a copper foil (current collector), dried at 80 °C for 10 h, and finally pressed under the pressure of 10 MPa. Afterward, the CR2016 coin-type cells were assembled in a highly pure argon-filled glovebox where both moisture and oxygen levels were less than 1 ppm. For LIBs, the lithium foils were used as the test electrodes, the metallic lithium counter/reference electrolyte, a polypropylene separator(Celgard 2400), and an electrolyte of 1 M $LiPF_6$ in ethylene carbonate and diethyl carbonate (EC/DMC, 1/1 vol). Cyclic voltammetry (CV) experiments were conducted by using a CHI 660E (Shanghai Chenhua Co. Ltd., China) electrochemical workstation at a scan rate of 0.5 mV s^{-1} between 0.005 V and 3 V vs. Li/Li^+. Charge-discharge measurements were carried out galvanostatically at a current density of 100 mA/g in the voltage range of 0.005–3.0 V using a battery test system (LAND CT2001A model, Wuhan Jinnuo Electronics. Ltd., China). Electrochemical impedance spectroscopy (EIS) were tested by using a CHI 660E electrochemical workstation in the frequency range of 1–10^5 Hz at the open circuit potential.

3. Results and discussion

3.1. Characterizations of the as-prepared samples

The compositions and crystal phases of the NiO/C hollow

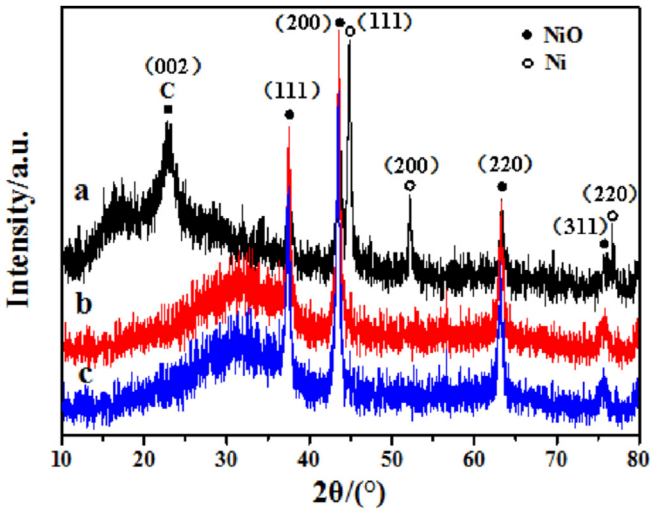

Fig. 1. XRD patterns of (a) NiO/C hollow microspheres, (b) NiO hollow microspheres and (c) NiO particles prepared without template.

microspheres, NiO hollow microspheres prepared with templates, and NiO particles prepared without templates were characterized by XRD, Fig. 1. All the diffraction patterns show peaks at 37.24°, 43.27°, 62.87° and 75.41° of 2θ, which can be assigned to the (111), (200), (220) and (311) crystal planes of the NiO (JCDPS # 47–1049). No additional peaks from the impurities are observed in the NiO patterns, demonstrating that the NiO samples prepared with and without templates are of high purity and good crystallinity. The observed diffraction peak at 22.76° can be assigned to the (002) crystal planes of C (JCDPS # 41–1487) in the NiO/C materials. However, the profile of C peaks is wide and not sharp, indicating poor crystallinity of C. Meanwhile, as for the NiO/C product, the observed three diffraction peaks at 44.507°, 51.846° and 76.370° of 2θ can be assigned to the (111), (200) and (220) crystal planes of Ni (JCDPS # 50–0926). The generation of Ni elementary substance may be caused by the redox reaction between C and NiO in N_2 atmosphere.

Fig. 2a shows the SEM images of the original morphology of yeast. The yeast is observed to be approximately spherical with the diameter ranging from 2 to 2.5 μm. Fig. 2b&c reveal the morphology of the NiO hollow microspheres before and after calcination at 600 °C. The calcined samples are observed to have

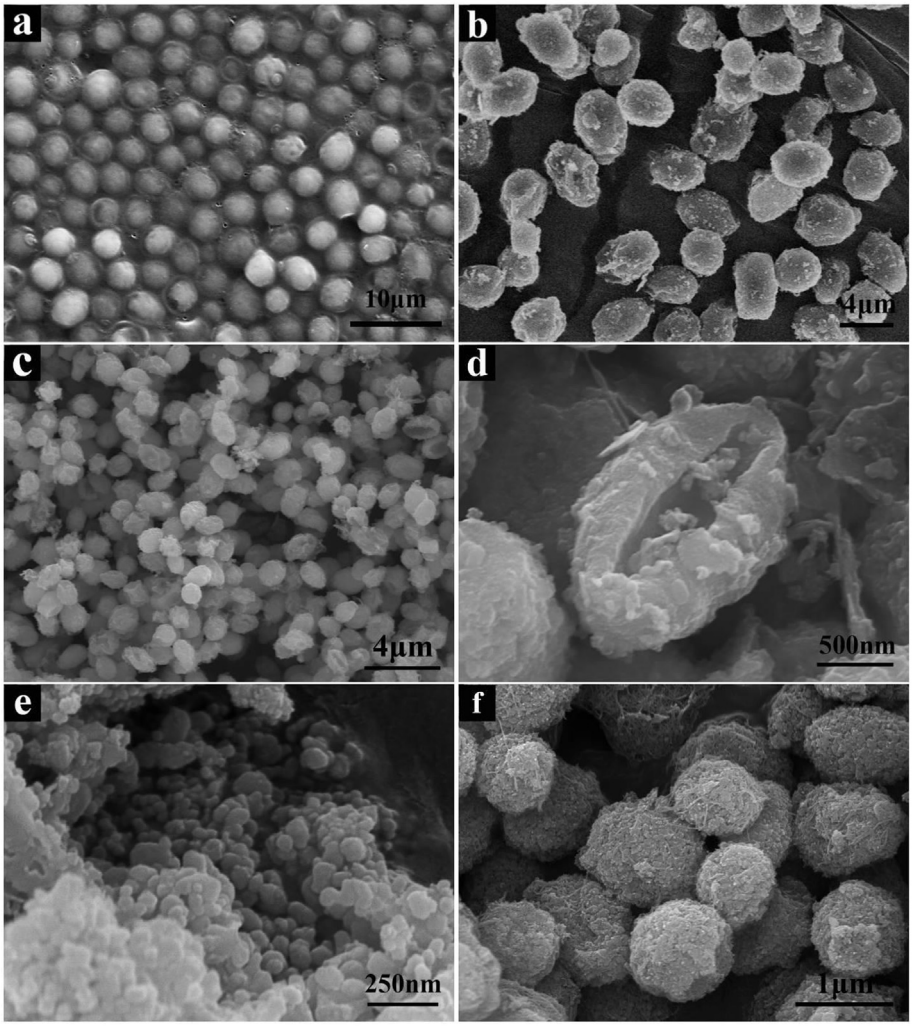

Fig. 2. SEM images of (a) yeast template, (b) NiO microspheres before calcination, (c) and (d) NiO hollow microspheres after calcination, (e) NiO particles prepared without yeast template and (f) NiO/C hollow microspheres.

retained the morphology of the yeast template even though the template was removed. The obtained NiO samples are observed relatively uniform nano structures with hollow interiors and with an averaged diameter ranging from 1.5 to 2 μm. A cracked hollow microsphere is shown in Fig. 2d, demonstrating the hollow structure of the samples. The diameter of the NiO hollow microspheres is smaller when compared to the products before calcination, which may be due to the removal of yeast template and the shrink of the NiO cell. Fig. 2e shows the SEM images of the NiO particles prepared without yeast templates. The as-prepared NiO products are small particles with the diameter around 50 nm. Meanwhile, Fig. 2f shows the SEM images of the NiO/C hollow microspheres. The microspheres also retain the spherical morphology of the templates with the diameter around 1 μm.

In agreement with the SEM results, the NiO hollow microsphere structure can be clearly observed from the TEM images and the shell thickness is around 500 nm, Fig. 3a. At the same time, Fig. 3b shows a low magnification TEM image of the NiO/C microspheres, the as-prepared NiO/C products are composed of small particles with the diameter around 40 nm, Fig. 3c. Fig. 3d shows the high resolution (HR) TEM image of NiO/C microspheres. The lattice-resolved image of NiO/C microspheres shows a lattice spacing of 0.209 nm, corresponding to the d-spacing of (200) crystal planes of NiO. But the lattice fringe of C is not observed, which is coincided with the XRD analysis of poor crystallinity of C.

Thermogravimetric analysis (TGA) of NiO/C was investigated and the result is shown in Fig. 4. The data illustrates the weight of examples has no obvious change below 400 °C, while a weight loss of approximately 30 wt% is due to the oxidation of carbon of NiO/C between 400 and 540 °C. Based on the analysis of TGA, the weight ratio of C and NiO in NiO/C composites is about 3:7.

The N_2 adsorption/desorption isotherms and the accumulated pore size distributions of NiO prepared without templates, NiO hollow microspheres and NiO/C hollow microspheres were investigated, as illustrated in Fig. 5. It is obvious that the N_2 adsorption/desorption of samples all exhibit the type IV nitrogen adsorption branch. The type-H3 hysteresis loop existing in isotherms reveals

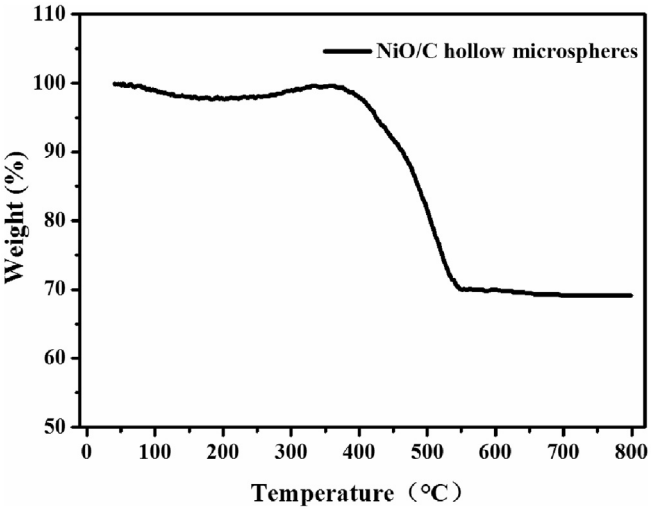

Fig. 4. TG pattern of NiO/C hollow microspheres.

the presence of mesopores in the all samples and the pore sizes are described in detail in the inset of Fig. 5. As shown in Table 1, it is found that NiO/C shows the largest surface area of 193.21 $m^2 g^{-1}$ which is found to be 15 times and 4 times larger than that of NiO prepared without templates and NiO hollow microspheres. Compared with NiO hollow microspheres, the decrease of pore size of NiO/C maybe attribute to the release of gas during the carbonization process.

3.2. *Influencing factors*

The factors such as the concentration of $Ni(NO_3)_2$, the calcination temperature and the aging time were observed to play important roles in the formation of special morphology and the crystal type of the NiO hollow microspheres. The $Ni(NO_3)_2$

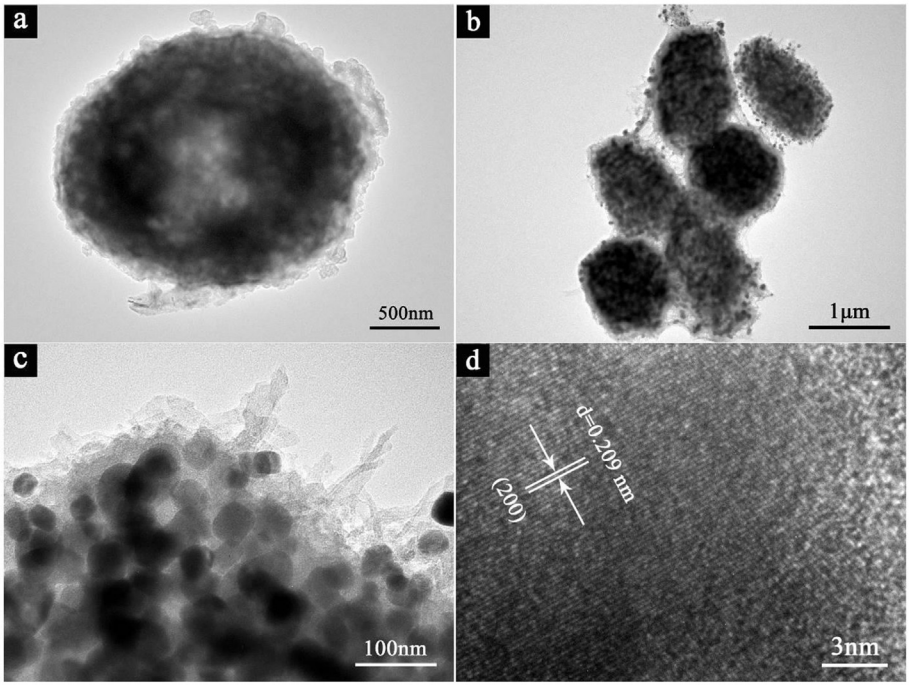

Fig. 3. TEM images of (a) NiO hollow microspheres, (b) and (c) NiO/C hollow microspheres, (d) HRTEM images of NiO/C hollow microspheres.

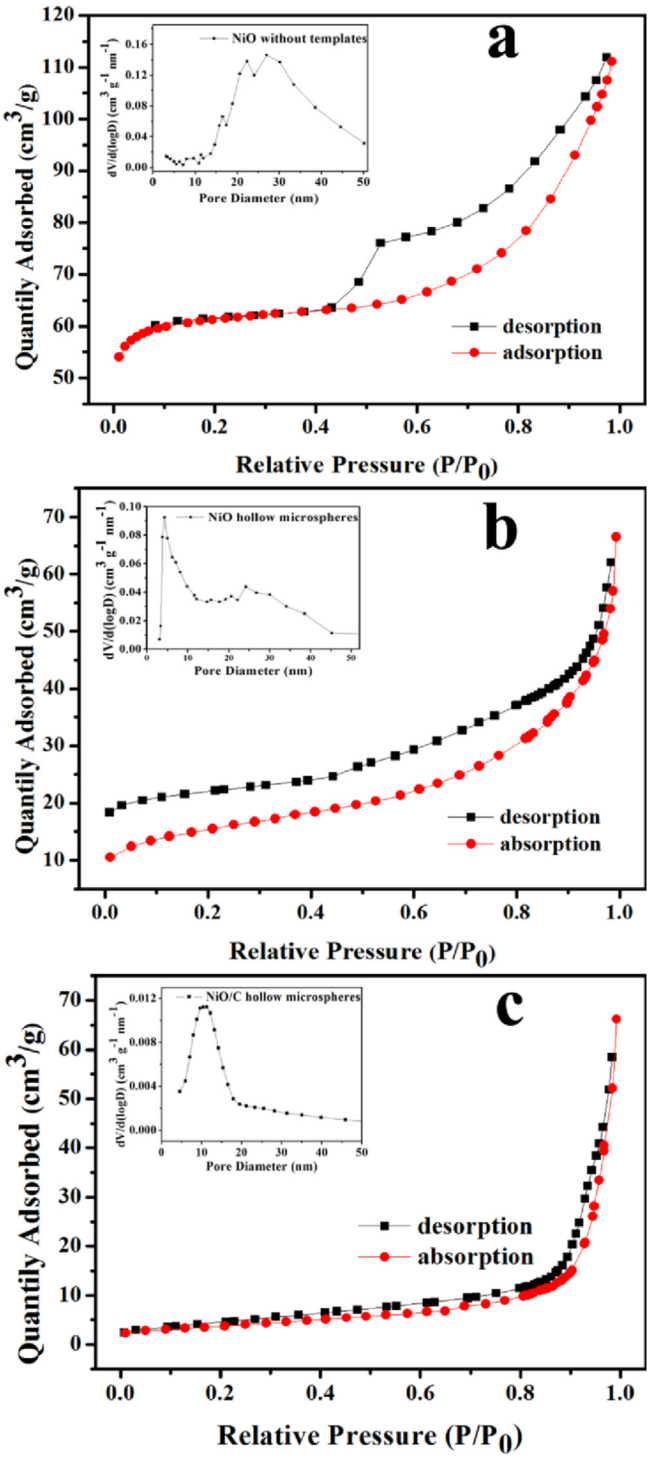

Fig. 5. N_2 sorption isotherms and accumulated pore size distribution: (a) NiO prepared without templates, (b) NiO hollow microspheres, (c) NiO/C hollow microspheres.

Table 1
BET surface area and pore volume of samples.

Samples	BET surface area ($m^2\ g^{-1}$)	Average pore size (nm)
NiO without templates	13.68	29.96
NiO hollow microspheres	50.68	4.12
NiO/C hollow microspheres	193.21	13.79

concentration was observed to play an essential role in controlling the morphology of the products. Uniform NiO hollow microspheres could be obtained at a concentration of 0.5 M, Fig. 6b. The molar ratio of $Ni(NO_3)_2$ and NH_4HCO_3 was always maintained at 1/1. When the concentration of $Ni(NO_3)_2$ was decreased to 0.25 M, no complete sphere was found, Fig. 6a. It might be because that the amount of Ni^{2+} was unable to coat the entire surface of the yeast templates, and the shell was not thick enough to maintain the spherical structure. However, when the concentration of $Ni(NO_3)_2$ was increased to 1 M, the yeast template lost its structure directing effect to the final product due to the high content of the salt solution, which lead to the NiO particles become agglomerated and cracked, Fig. 6c.

The influence of the calcination temperature on the crystal phases of the products was investigated under a calcination time of 2 h. As shown in Fig. 7, the XRD patterns (Fig. 7d) shows the as-prepared sample presents broad diffraction bands, indicating its poor crystallinity at <600 °C. After calcined at 600 °C for 2 h, diffraction peaks become pronounced and the diffraction peaks at 37.24°, 43.27°, 62.87° and 75.41° can be assigned to the (111), (200), (220) and (311) crystal planes of the NiO (JCDPS # 47–1049). This is because that the crystallization degree of sample grows as the increase of temperature. At 300–450 °C, the sample is mainly amorphous due to relatively small degree of crystallization, resulting the samples showed poor crystallinity. As the temperature increase, the crystallization degree of crystal increases, which resulted better degree of crystallinity at 600 °C [49]. Meanwhile, it is illustrated clearly in Fig. 7a, b and c that the NiO hollow microspheres obtained at a calcination temperature of 450 °C and 600 °C show an averaged diameter ranging from 1.5 to 2 μm which is found to be significantly smaller than the diameter from 2 to 3 μm of products calcined at 300 °C. The changes of diameter of samples can be attributed to the greater degree of carbonization yeast at high calcination temperature to reduce the volume of NiO to a greater extent.

Fig. 8 shows the SEM images of the products from different ageing time while keeping all other parameters identical. The NiO microspheres with uniform size could be obtained when the ageing time was less than 12 h, Fig. 8 a&b. When prolonging the aging time to 24 h, the NiO microspheres become irregular and imperfect. With increasing the aging time, the NiO microspheres tend to be uniform. The reason might be that when aging time is overlong, the yeast cells will shrink because of water loss, leading to dents or damage on the surface of NiO particles.

3.3. Formation mechanism

From the observed XRD, SEM and TEM results, the possible pathway for the formation of the NiO/C hollow microspheres was proposed. The whole process mainly undergoes the following four stages as shown in Scheme 1. Firstly, there are many reactive functional groups on the cell wall of the yeast, such as carboxyl and hydroxyls groups which are able to bind mental cations through coordination or electrostatic attractions. When $Ni(NO_3)_2 \cdot 6H_2O$ was added into the yeast aqueous solution and stirred for 1 h at room temperature, the yeast would gradually adsorbed Ni^{2+} through the coordination or electrostatic attractions between the inherent functional groups on the cell walls and Ni^{2+} from $Ni(NO_3)_2 \cdot 6H_2O$ solution. The yeast served as a hard template to direct the hollow microsphere morphology of the products. In the second-step, the yeast/$Ni(OH)_2$ core-shell spheres were formed when NH_4HCO_3 was added to the system. After this process, the resultant yeast/$Ni(OH)_2$ core-shell spheres had a morphology very similar to the yeast template. Thirdly, after calcination, the yeast/$Ni(OH)_2$ core-shell spheres were converted to NiO hollow microspheres, and the NiO

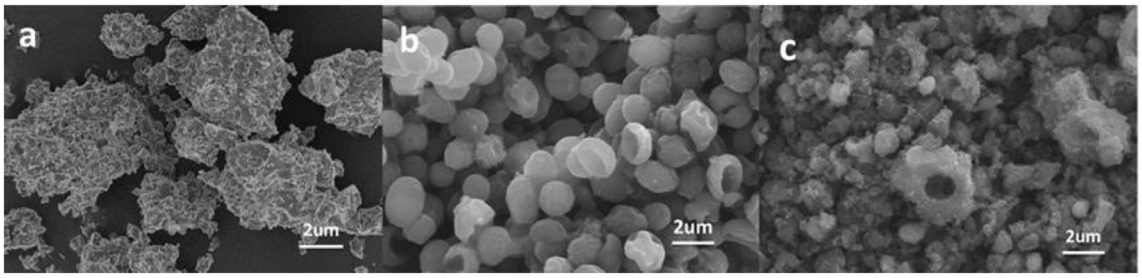

Fig. 6. SEM images of the NiO products obtained with a $Ni(NO_3)_2$ concentration of (a) 0.25, (b) 0.5, and (c) 1 M.

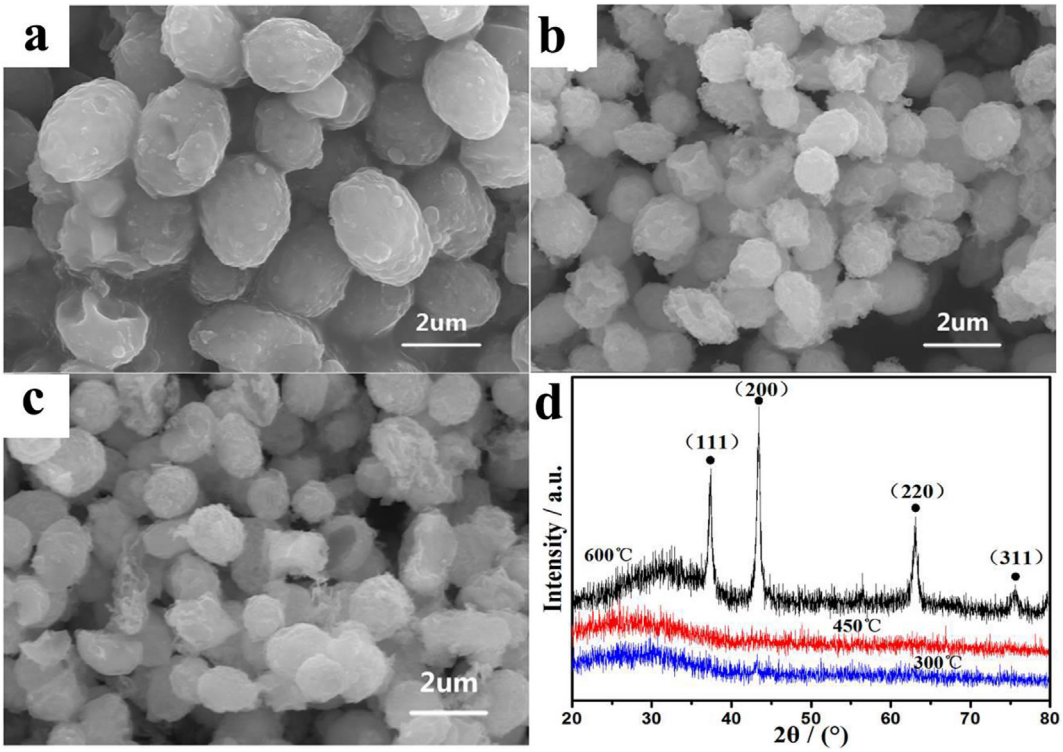

Fig. 7. SEM images of the NiO products calcined at (a) 300, (b) 450, and (c) 600 °C and (d) XRD patterns of the NiO products gained at different temperature.

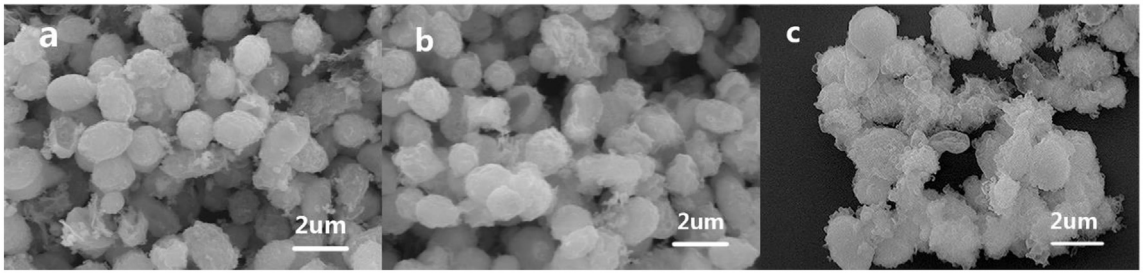

Fig. 8. SEM images of the products from an ageing time of (a) 6, (b) 12, and (c) 24 h.

hollow microspheres retained the original morphologies of the yeast templates. At the same time, along with the ashing of the yeast template, the volume of the as-prepared NiO hollow microspheres was slowly contracting inward. Finally, the NiO/C hollow microspheres were synthesized via a hydrothermal method by using glucose as the carbon source.

3.4. Electrochemical performance in LIBs

To investigate the electrochemical performance of the NiO/C hollow microspheres as an anode for lithium ion batteries, discharge/charge cycling was carried out in the voltage range of 0.005–3.0 V (vs Li/Li^+) at a current density of 100 mA/g at room

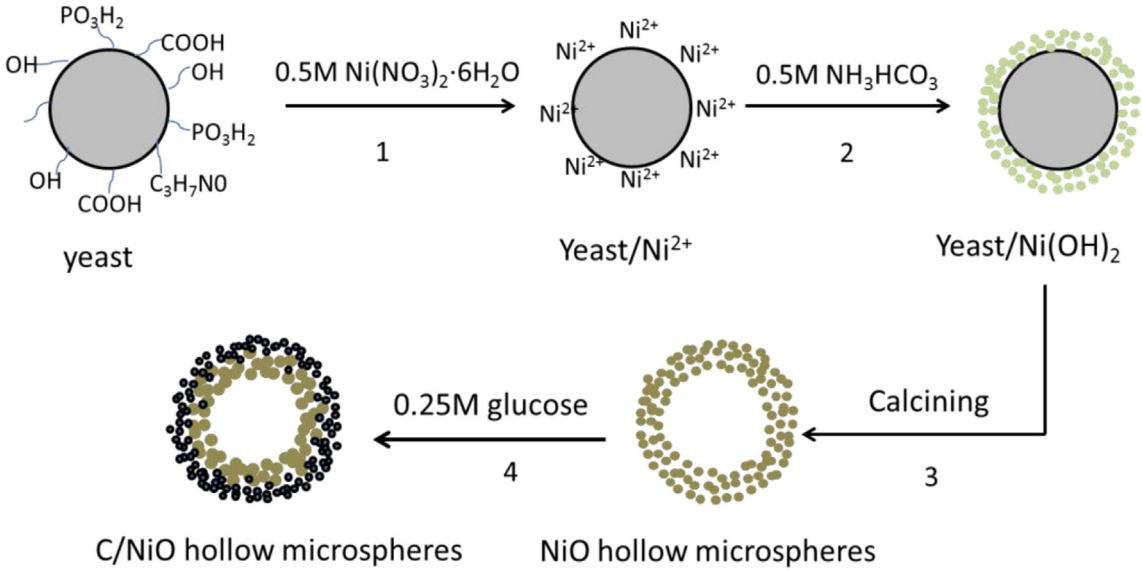

Scheme 1. Schematic illustration of proposed formation mechanism of NiO/C hollow microspheres.

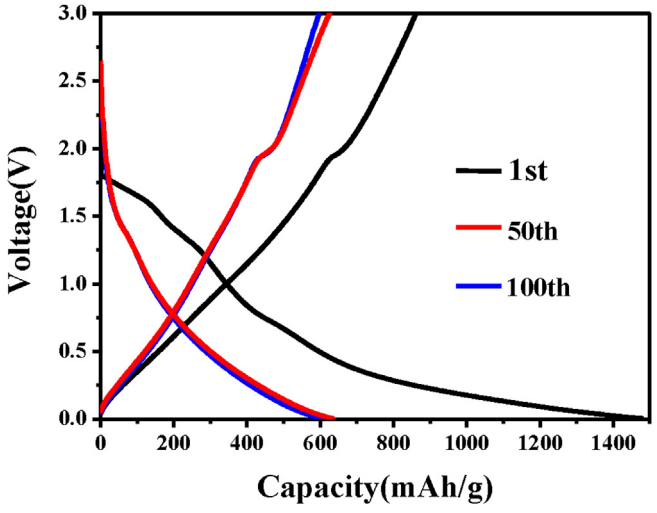

Fig. 9. Charge/discharge profile of the NiO/C hollow microspheres.

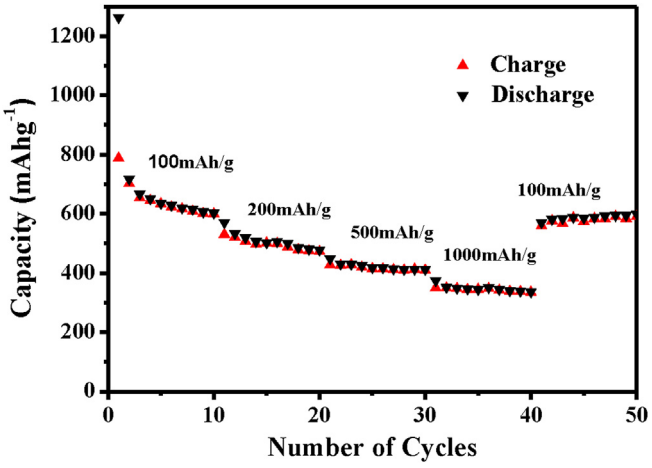

Fig. 10. Rate performance of the NiO/C hollow microspheres.

temperature. Fig. 9 shows the typical charge/discharge profiles of the as-prepared NiO/C hollow microspheres in the 1st, 50th and 100th cycles. The shape of the profiles did not change significantly during the cycling, indicating good stability of the NiO/C hollow microspheres as an anode. In the first discharge process, the constant slops at 0.7 V indicates the initial reduction of Ni^{2+} to Ni^0 and the formation of a partially reversible solid electrolyte interface (SEI) layer, consistent with the literature reported [50]. At the same time, a plateau at ~2.0 V is observed, Fig. 9. These plateaus are due to the reversible oxidation/reduction of Ni/NiO and Li/Li_2O during the Li^+ insertion/extraction [51]. The relative reactions are presented as follows [52,53]:

$$NiO + 2Li \rightleftharpoons Ni + Li_2O \quad (1)$$

Rate performance is another important precondition to apply as anode material in Li-ion batteries. Therefore, the as-prepared NiO/C hollow microspheres were examined with different current densities, Fig. 10. Each step comprised of 10 charge/discharge cycles at different current density from 100 to 1000 mA/g. The results show that the as-obtained NiO/C hollow microspheres keep a discharge capacity of 602, 478 and 412 mAh/g at a current density of 100, 200 and 500 mA/g, respectively. It should be noticed that even at an extremely high current density of 1000 mA/g after 10 cycles, the discharge capacity still remains at 336 mAh/g. At the same time, when the current rate is turned back to low current rate (such as 100 mA/g), the discharge capacity can be recovered to 599 mAh/g, 99% retention of the initial capacity. The results indicate that the as-prepared NiO/C hollow microspheres can tolerate high current charge/discharge cycling and meet the requirements of LIBs for the fast charge and discharge.

In order to investigate the electrochemical properties of the NiO materials, cyclic voltammetry (CV) curves with a potential range of 0.005–3 V vs. Li/Li^+ at a scan rate of 0.5 mV s^{-1} and Electrochemical impedance spectroscopy (EIS) tests in the frequency range of 1–10^5 Hz after 100 cycles at a current rate of 100 mA g^{-1} were carried out, respectively. The result of CV curves is shown in Fig. 11. The peak locating at approximately 0.7 V in negative scanning process corresponds to the initial reduction of NiO to Ni accompanied with the formation of Li_2O, while the peak in 2.3 V reveals the oxidation of Ni^0 to Ni^{2+} along with the decomposition of Li_2O.

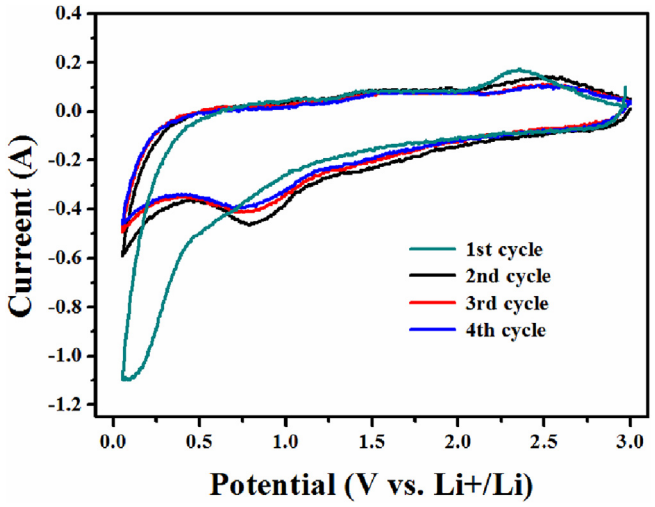

Fig. 11. CV curves of NiO/C hollow microspheres at a scanning rate of 0.5 mV s^{-1}.

Below ~0.5 V, there is a steep voltage drop, which is attributed to electrolyte decomposition accompanied with the formation of SEI film formation. A shark peak appears near 0 V, which is related to Li^+ insertion into the carbon layer. Moreover, the CV curves are stable and well overlapped after 2nd cycle, indicating high electrochemical reversibility and good capacity retention for the NiO/C microspheres electrodes.

As it is shown in Fig. 12, the discharge capacity for all the as-prepared NiO materials droped rapidly in the first cycle due to the formation of amorphous Li_2O matrix and intense surface reactions with the Li—Ni compounds and the electrolyte solution [54]. From the second cycle to the 100th cycle, the NiO/C hollow microspheres and NiO hollow microspheres showed a highly reversible behavior compared with the NiO particles prepared without the yeast template. In the second cycle, the NiO/C and NiO hollow microspheres exhibited a discharge capacity of 760 and 785 mAh/g, respectively, which are higher than the NiO particles (345 mAh/g). From Fig. 9, when compared with the NiO hollow microspheres, the discharge capacity of the NiO/C hollow microspheres is observed lower before 25 cycles, that may be caused by the lower capacity of carbon [55]. But, after 25 cycles, the advantages of NiO/C hollow microspheres in electrochemical

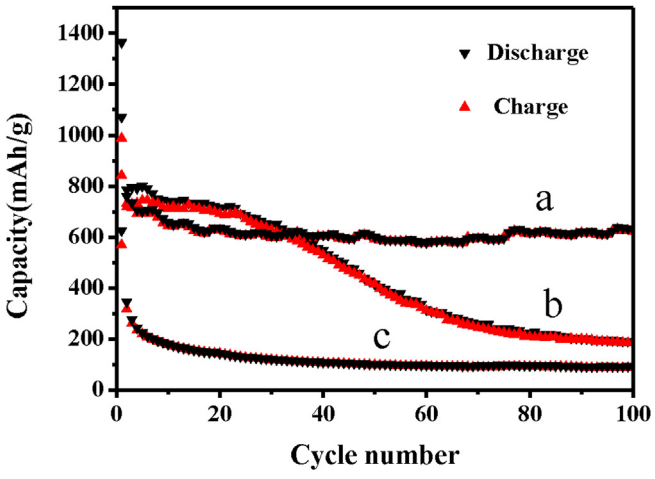

Fig. 12. The cycle performance of (a) NiO/C hollow microspheres, (b) NiO hollow microspheres and (c) NiO particles prepared without templates.

performances are gradually appearing. At the 100 cycles, the discharge capacity of NiO/C microspheres is 628 mAh/g, which is about 100% retention of the reversible capacity of the 25th. However, the discharge capacity of NiO hollow microspheres is only 191 mAh g^{-1}, which is just about 28% retention of the reversible capacity of the 25th. Thus, it can be seen that the NiO/C microspheres exhibit superior discharge capacity and cycling performance. The carbon coated NiO microspheres with an internal hollow structure and approximate sphere shape can help to build a better conductive network which can provide structural stability for volume change and promote the electron transfer during the lithiation and delithiation process. And the improved performance observed also should be attributed to good dispersion which can make the as-prepared product have a good contact with the electrolyte. During the charge/discharge process, the Li^+ ions would be able to diffuse and react with the NiO product easily, leading to the enhanced electrochemical performance as anode materials for LIBs.

The Nyquist plots of samples are shown in Fig. 13, which exhibit the same tendency including a semicircle followed by a slanted straight line. A semicircle at a high frequency due to a parallel combination of electrical double layer capacitance (Cdl) and activation resistance from kinetic effect are related to charge transfer resistance (R_{ct}) and the surface film resistance (R_{sf}). The slant at low-frequency region is due to diffusion of Li^+ in the bulk of the electrode corresponding to Warburg impedance (Z_W). Electrolyte resistance (R_e) can be measured according to the intercept at a very high frequency region. The data in Table 2 reveals that the R_{ct} value of NiO/C hollow microspheres of 185 Ω is smaller than that of NiO of 252 Ω and NiO without templates of 453 Ω, which can be explained by the significant enhancement of electronic conductivity of NiO/C composite electrode prepared by coating of a layer of conducting carbon on the non-conducting NiO particles. That the NiO/C hollow microspheres show the largest slope of three samples

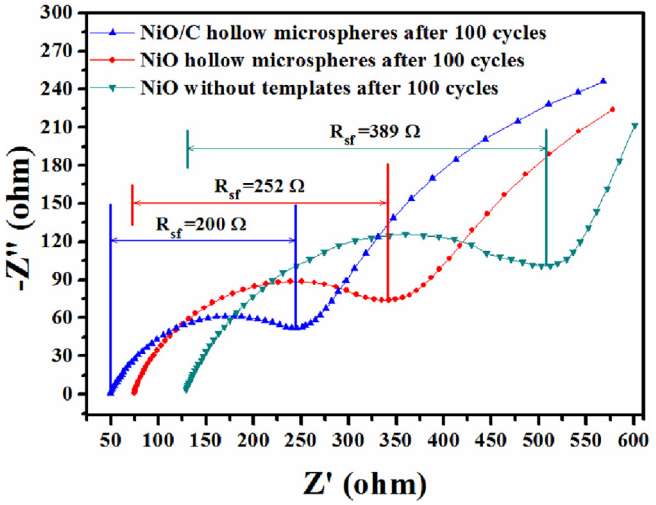

Fig. 13. Nyquist plot of NiO/C hollow microspheres, NiO hollow microspheres, NiO without templates after 100 cycles.

Table 2
R_e, R_{sf} and R_{ct} of samples.

Samples	R_e (Ω)	R_{sf} (Ω)	R_{ct} (Ω)
NiO without templates	129	389	453
NiO	74.5	252	252
NiO/C	49.3	200	185

in the low-frequency region illustrates the improvement of diffusion of lithium ion in the electrode. Therefore, the electrochemical performance of particles can be significantly enhanced by using yeast to prepared and coating carbon on its surface.

4. Conclusion

A facile bio-template method to prepare NiO/C hollow microspheres was reported. The as-prepared product maintained the morphology of yeast templates very well with a uniform diameter of 1.5–2.0 μm. The parameters including the concentration of [$Ni(NO_3)_2 \cdot 6H_2O$], the calcination temperature and the aging time can affect the morphology and crystal type of the NiO microspheres. The electrochemical test results show that when compared with the NiO hollow microspheres and NiO particles prepared without templates, the NiO/C hollow microspheres exhibit a better cycling stability. This synthesis method may provide a facile, economic, and green strategy for the preparation of other metal oxides with hollow microspheres structure, and the better Li-storage performance implies that the as-prepared NiO/C hollow microspheres are promising anode materials for highly efficient LIBs.

References

[1] T. Li, X. Li, Z. Wang, H. Guo, A short process for the efficient utilization of transition-metal chlorides in lithium-ion batteries: a case of $Ni_{0.8}Co_{0.1}Mn_{0.1}O_{1.1}$ and $LiNi_{0.8}Co_{0.1}Mn_{0.1}O_2$, J. Power Sources 342 (2017) 495–503.

[2] H. Zhang, H. Osgood, X. Xie, Y. Shao, G. Wu, Engineering nanostructures of PGM-free oxygen-reduction catalysts using metal-organic frameworks, Nano Energy 31 (2017) 331–350.

[3] H. Ge, H. Hao, H. Osgood, B. Zhang, L. Chen, Advanced mesoporous spinel $Li_4Ti_5O_{12}$/rGO composites with increased surface lithium storage capability for high-power lithium-ion batteries, ACS Appl. Mater. Inter. 14 (2016) 9162–9169.

[4] S. Guo, J. Liu, S. Qiu, Y. Mang, X. Yan, Enhancing electrochemical performances of TiO_2 porous microspheres through hybridizing with $FeTiO_3$ and nanocarbon, Electrochim. Acta 7 (2016) 556–565.

[5] Y. Feng, X. Jiang, E. Ghafari, B. Kucukgok, C. Zhang, Metal oxides for thermoelectric power generation and beyond, Adv. Compos. Hybrid Mater. (2017) 1–13, https://doi.org/10.1007/s42114-017-0011-4 in press.

[6] X. Ma, P. Kolla, R. Yang, W. Zhang, Y. Zhao, Electrospun polyacrylonitrile nanofibrous membranes with varied fiber diameters and different membrane porosities as lithium-ion battery separators, Electrochim. Acta 236 (2017) 417–423.

[7] C. Alippi, A unique timely moment for embedding intelligence in applications, CAAI Transactions on Intelligence Technology, CAAI Trans. Intellig. Technol. 1 (2016) 1–3.

[8] H. Jin, Q. Chen, Z. Chen, Y. Hu, J. Zhang, Multi-LeapMotion sensor based demonstration for robotic refine tabletop object manipulation task, CAAI Trans. Intellig. Technol. 1 (2016) 104–113.

[9] X. Zhang, H. Gao, G. Guo, G. Li, Y. Liu, A study on key technologies of unmanned driving, CAAI Trans. Intellig. Technol. 1 (2016) 4–13.

[10] S. Padhy, S. Panda, A hybrid stochastic fractal search and pattern search technique based cascade PI-PD controller for automatic generation control of multi-source power systems in presence of plug in electric vehicles, CAAI Trans. Intellig. Technol. 2 (2016) 12–25.

[11] N. Wu, J. Qiao, J. Liu, W. Du, D. Xu, Strengthened electromagnetic absorption performance derived from synergistic effect of carbon nanotube hybrid with Co@ C beads, Adv. Compos. Hybrid Mater. (2017) 1–11, https://doi.org/10.1007/s42114-017-0008-z in press.

[12] K. Zhang, G.H. Li, L.M. Feng, N. Wang, J. Guo, Ultralow percolation threshold and enhanced electromagnetic interference shielding in poly (l-lactide)/multi-walled carbon nanotube nanocomposites with electrically conductive segregated networks, J. Mater. Chemc 36 (2017) 9359–9369.

[13] C. Jia, P. Yang, H.S. Chen, J. Wang, Template-free synthesis of mesoporousanatasetitania hollow spheres and their enhanced photocatalysis, CrystEngComm 15 (2015) 2940–2948.

[14] N. Sharma, H. Ojha, A. Bharadwaj, D.P. Pathak, R.K. Sharma, Preparation and catalytic applications of nanomaterials: a review, RSC Adv. 66 (2015) 53381–53403.

[15] Z. Sun, L. Zhang, F. Dang, Y. Liu, Z. Fei, Experimental and simulation-based understanding of morphology controlled barium titanate nanoparticles under co-adsorption of surfactants, CrystEngComm 19 (2017) 3288–3298.

[16] L. Zhang, W. Yu, C. Han, J. Guo, Q. Zhang, Large scaled synthesis of heterostructured electrospun TiO2/SnO2 nanofibers with an enhanced photocatalytic activity, J. Electro. Chem. Soc. 9 (2017) 651–656.

[17] X. Xiang, F. Pan, Y. Li, A review on adsorption-enhanced photoreduction of carbon dioxide by nanocomposite materials, Adv. Compos. Hybrid Mater. (2017) 1–26, https://doi.org/10.1007/s42114-017-0001-6 in press.

[18] Y.Y. Fan, D.X. Han, Z.Q. Song, Z.H. S, X.D. D, Regulations of silver halide nanostructure and composites on photocatalysis, Adv. Compos. Hybrid Mater. (2017) 1–31, https://doi.org/10.1007/s42114-017-0005-2 in press.

[19] J. Huang, Y. Cao, Q. Shao, X. Peng, Z. Guo, Magnetic nanocarbon adsorbents with enhanced hexavalent chromium removal: morphology dependence of fibrillar vs particulate structures, Ind. Eng. Chem. Res. 38 (2017) 10689–10701.

[20] C. Yan, F. Rosei, Hollow micro/nanostructured materials prepared by ion exchange synthesis and their potential applications, New J. Chem. 5 (2014) 1883–1904.

[21] Y. Liu, J. Goebl, Y. Yin, Templated synthesis of nanostructured materials, Chem. Soc. Rev. 7 (2014) 2610–2653.

[22] Z. Zhang, M.J. Zaworotko, Template-directed synthesis of metal–organic materials, Chem. Soc. Rev. 16 (2014) 5444–5455.

[23] R. Balgis, T. Ogi, A.F. Arif, G.M. Anikumar, T. Mori, Morphology control of hierarchical porous carbon particles from phenolic resin and polystyrene latex template via aerosol process, Carbon 84 (2014) 281–289.

[24] M. LindoA, E. Pellicer, M.A. Zeeshan, R. Grisch, F. Qiu, The biocompatibility and anti-biofouling properties of magnetic core–multishellFe@C NWs–AAO nanocomposites, Phys. Chem. Chem. 20 (2015) 13274–13279.

[25] Y.K. Hong, B.H. Kim, I.K. Dong, H.P. Dong, J. Joo, High-yield and environment-minded fabrication of nanoporous anodic aluminum oxide templates, RSC Adv. 34 (2015) 26872–26877.

[26] W.X. Zhu, S.S. Ge, Q. Shao, Adsorption properties of ZrO_2 hollow microboxes prepared using $CaCO_3$ cubes as templates, RSC Adv. 6 (2014) 81736–81743.

[27] W.X. Zhu, S.S. Ge, Q. Shao, Fabrication and characterization of hollow zirconia microspheres using calcium carbonate as template, Z. Phys. Chem. 11 (2016) 1617–1628.

[28] K.M. Nam, J.T. Park, Chemical approach to a new crystal structure: phase control of manganese oxide on a carbon sphere template, Chem. Asian J. 12 (2014) 3525–3532.

[29] X. Sun, J. Liu, Y. Li, Use of carbonaceous polysaccharide microspheres as templates for fabricating metal oxide hollow spheres, Chem. Enr. J. 7 (2006) 2039–2047.

[30] J. Huang, L. Lin, D. Sun, H. Chen, D. Yang, Bio-inspired synthesis of metal nanomaterials and applications, Chem. Soc. Rev. 17 (2015) 6330–6374.

[31] S. Ge, Q. Zhang, X. Wang, Q. Shao, L. Bao, Bacteria-directed construction of ZnO/CdS hollow rods and their enhanced photocatalytic activity, J. Nanosci. Nanotechnol. 5 (2016) 4929–4935.

[32] A.H. Lim, H.W. Shim, S.D. Seo, G.H. Lee, K.S. Park, Biomineralized Sn-based multiphasic nanostructures for Li-ion battery electrodes, Nanoscale 15 (2012) 4694–4701.

[33] H. Yang, M. Du, T. Odoom-Wubah, Microorganism-mediated, CTAB-directed synthesis of hierarchically branched au-nanowire/Escherichia coli nanocomposites with strong-nearinfraredabsorbance, J. Chem. Technol. Biot. 9 (2014) 1410–1418.

[34] T. Li, J. Wang, Z. Wang, H. Guo, Y. Li, A new design concept for preparing nickel-foam-supported metal oxide microspheres with superior electrochemical properties, J. Mater. Chem. A 5 (2017) 14996–15001.

[35] R. SohnJ, J.S. Han, Preparation and characterization of NiO/CeO_2-ZrO_2/WO_3 catalyst for acid catalysis, J. Ind. Eng. Chem. 3 (2005) 439–448.

[36] W. Zhou, L. Guo, Iron triad (Fe, Co, Ni) nanomaterials: structural design, functionalization and their applications, Chem. Soc. Rev. 46 (2015) 6679–6707.

[37] J. Adhikary, P. Chakraborty, B. Das, A. Datta, S.K. Dash, Preparation and characterization of ferromagnetic nickel oxide nanoparticles from three different precursors: application in drug delivery, RSC Adv. 45 (2015) 35917–35928.

[38] G.A. Niklasson, C.G. Granqvist, Electrochromics for smart windows: thin films of tungsten oxide and nickel oxide, and devices based on these, J. Mater. Chem. 2 (2017) 127–156.

[39] Z. Yan, Q. Hu, G. Yan, H. Li, K. Shin, Co_3O_4/Co nanoparticles enclosed graphitic carbon as anode material for high performance Li-ion batteries, Chem. Eng. J. 321 (2017) 495–501.

[40] J. Leng, Z. Wang, X. Li, H. Guo, H. Li, Accurate construction of hierarchical nickel-cobalt oxide multishell yolk-shell structure with large and ultrafast lithium storage capability, J. Mater. Chem. A 5 (2017) 13469–13474.

[41] P. Poizot, S. Laruelle, S. Grugeon, L. Dupont, J. Tarascon, Nano-sized transition-metal oxides as negative-electrode materials for lithium-ion batteries, Nature 6806 (2000) 496–499.

[42] X.H. Huang, J.P. Tu, C.Q. Zhang, J.Y. Xiang, Net-structured NiO–C nanocomposite as Li-intercalation electrode material, Electrochem. Commun. 5 (2007) 1180–1184.

[43] C. Lin, L. Hu, C. Cheng, K. Sun, X. Guo, Q. Shao, J. Li, N. Wang, Z. Guo, Nano-$TiNb_2O_7$/carbon nanotubes composite anode for enhanced lithium-ion storage, Electrochim. Acta 260 (2018) 65–72.

[44] X. Lou, C. Lin, Q. Luo, J. Zhao, B. Wang, J. Li, Q. Shao, X. Guo, N. Wang, Z. Guo, Crystal-structure modification enhanced $FeNb_{11}O_{29}$ anodes for lithium-ion batteries, ChemElectroChem 4 (2017) 3171–3180.

[45] W. Zhou, J.L. Zheng, Y.H. Yue, L. Guo, Highly stable rGO-wrapped Ni_3S_2 nanobowls: structure fabrication and superior long-life electrochemical performance in LIBs, Nano Energy 11 (2015) 428–435.

[46] T. Liu, C. Jiang, B. Cheng, W. You, J. Yu, Hierarchical flower-like C/NiO composite hollow microspheres and its excellent supercapacitor performance, J. Power Sources 359 (2017) 371–378.
[47] Y. Yang, F. Yang, H. Hu, S. Lee, Y. Wang, Dilute NiO/carbon nanofiber composites derived from metal organic framework fibers as electrode materials for supercapacitors, Chem. Eng. J. 307 (2017) 583–592.
[48] B. Zhao, Q. Shao, L. Hao, L. Zhang, Z. Liu, Yeast-template synthesized Fe-doped cerium oxide hollow microspheres for visible photodegradation of acid orange 7, J. Colloid Inter. Sci. 511 (2018) 39–47.
[49] S. Bai, H. Fu, R. Luo, A. Chen, NiO hierarchical hollow microspheres doped Fe to enhance triethylamine sensing properties, Mater. Lett. 210 (2018), 308–305.
[50] D. Xie, W. Yuan, Z. Dong, Q. Su, J. Zhang, Facile synthesis of porous NiO hollow microspheres and its electrochemical lithium-storage performance, Electrochim. Acta 92 (2013) 87–92.
[51] Y. Chen, R. Cai, Y. Yang, C. Liu, A. Yuan, Cyanometallic frameworks derived hierarchical porous Fe_2O_3/NiO microflowers with excellent lithium-storage property, J. Alloy Compd. 698 (2017) 469–475.
[52] Z. Li, L. Wei, Y. Liu, Y. Su, X. Dong, Facile synthesis of single-crystalline mesoporous NiO nanosheets as high-performance anode materials for Li-ion batteries, J. Mater. Sci-Mater. El. 2 (2017) 1–8.
[53] L. Zhang, J. Mu, Z. Wang, G. Li, Y. Zhang, One-pot synthesis of NiO/C composite nanoparticles as anode materials for lithium-ion batteries, J. Alloy Compd. 671 (2017) 60–65.
[54] J. Liang, Y. Zhao, L. Guo, Flexible free-standing graphene/SnO_2 nanocomposites paper for Li-ion battery, ACS. Appl. Mater. Inter. 11 (2012) 5742–5748.
[55] Y. Huang, X. Huang, J. Lian, D. Xu, L. Wang, Self-assembly of ultrathin porous NiO nanosheets/graphene hierarchical structure for high-capacity and high-rate lithium storage, J. Mater. Chem. 7 (2012) 2844–2847.